Regular paper

Constant absolute bandwidth six-pole quasi-elliptic tunable bandpass filter using synchronously tuned dual-mode resonators

Girdhari Chaudhary [a], Yongchae Jeong [b],*

[a] *JIANT-IT Human Resource Development Center, Jeonbuk National University, Jeonju-si, Republic of Korea*
[b] *Division of Electronic Engineering, Jeonbuk National University, Jeonju-si, Republic of Korea*

A B S T R A C T

This paper presents the design of a 6th-order tunable bandpass filter (BPF) that achieves constant absolute bandwidth (ABW) and transmission zeros (TZs) across a wide frequency tuning range. The proposed tunable BPF employs three synchronously tuned dual-mode resonators, along with a frequency-dependent coupling structure realized using a T-network consisting of series and shunt capacitors. To achieve constant ABW, the tunable external quality factors are implemented using series capacitor and shunt varactor. As an illustrative example, a 6th-order BPF is fabricated and measured, results revealing that the center frequency of BPF can be tuned from 1.39 GHz to 1.81 GHz (26.25 %) with two TZs on the lower and upper side of the passband, 1-dB constant ABW of 62 ± 1.5 MHz and return loss > 12 dB in every tuning state.

1. Introduction

Frequency tunable bandpass filters (BPFs) with a quasi-elliptic frequency response and constant absolute bandwidth (ABW) are highly desirable microwave components in microwave wireless communication systems [1]. Over the past decades, various designs of dual-mode tunable BPFs have been presented, each with unique functionalities such as center frequency and bandwidth control [2–5]. However, the majority of previously reported planar tunable BPFs with quasi-elliptic response and constant ABW have only focused on 2nd- and 3rd-order filter designs [6–13].

Designing higher-order quasi-elliptic tunable BPF that can operate with a constant ABW across a wide frequency tuning range (FTR) is a challenging task. In previous studies [14–17], 4th-order tunable BPFs with transmission zeros (TZs) are presented using varactor-tuned microstrip line resonators. However, these tunable BPFs are unable to achieve constant ABW while tuning the center frequency. In [18], quasi-elliptic tunable BPF is demonstrated using tri-mode resonator, however, large number of bias voltage control are necessary to achieve constant ABW. A fully reconfigurable dual-mode BPF is demonstrated in [19] using substrate integrated circular cavity resonator, however, frequency selectivity characteristics are poor. More recently, there have been reports of 4th- and 6th-order quasi-elliptic tunable BPFs with constant ABW [20–24]. In [20], 4th-order quasi-elliptic tunable BPF is demonstrated

using electric and magnetic cross-coupling. In [21] and [22], a synthesis of 4th-order tunable BPF with quasi-elliptic response and constant ABW is presented using element-variable coupling matrix (EVCM). In [23], a 6th-order microstrip line tunable BPF with quasi-elliptic response and constant ABW is presented by using a coupling matrix and frequency-curve shape design approach. Similarly, a 6th-order wideband tunable BPF with quasi-elliptic response and constant ABW is demonstrated in [24] using varactor-loaded $\lambda/2$ resonators and alternate *J/K* inverters.

In this paper, we propose a design of 6th-order microstrip line tunable BPF that achieves constant ABW across a wide FTR. The proposed design incorporates three synchronously tuned dual-mode resonators. To achieve constant ABW, we propose and analyze frequency-dependent coupling coefficients and external *Q*-factors.

2. Design theory

a) Coupling matrix analysis for quasi-elliptic response

Fig. 1(a) depicts the coupling diagram for 6th-order tunable BPF with quasi-elliptic response, where solid line and dotted line represent main coupling ($M_{s1} = M_{6L}$, $M_{12} = M_{56}$, $M_{23} = M_{45}$, and M_{34}) and cross-coupling between resonators (M_{14} and M_{36}), respectively. To achieve quasi-elliptic response, the transmission zeros (TZs) are generated at the lower side and upper sides of passband due to cross-coupling (M_{14}) between resonators 1 and 4, and cross-coupling (M_{36}) between

resonators 3 and 6. To reduce the number of resonators in the proposed 6th-order of tunable BPF, resonators 1 and 2, resonators 3 and 4, and resonators 5 and 6, are implemented using three dual-mode resonators R_1, R_2, and R_3, respectively.

To achieve tunable BPF frequency response with constant ABW, the even and odd-mode resonant frequencies (f_{ei} and f_{oi}) of dual-mode resonators play an important role where separation between them should be constant desired value (i.e. f_{oi}-$f_{ei} \cong f_{BW}$). Therefore, even and odd-mode resonant frequencies of dual-mode resonators R_1 and R_3 should be determined as (1) to achieve tunable frequency response with constant ABW.

$$f_{e1,3} = f_c - ABW \times M_{12} \tag{1a}$$

$$f_{o1,3} = f_c + ABW \times M_{12} \tag{1b}$$

where f_c is tunable passband center frequency and ABW is constant absolute bandwidth of filter. Similarly, even and odd-mode resonant frequencies of dual-mode resonator R_2 should be determined as (2).

$$f_{e2} = f_c - ABW \times M_{34} \tag{2a}$$

$$f_{o2} = f_c + ABW \times M_{34} \tag{2b}$$

Once even and odd-mode resonant frequencies are determined, coupling between dual-mode resonators ($k_{i,i+1}$), and external Q-factor (Q_{exe}) should be determined using (3).

$$k_{i,i+1} = \frac{ABW}{f_c} \times M_{i,i+1}, i = 2, 4, \cdots \tag{3a}$$

$$Q_{exe} = \frac{Q_e + Q_o}{2} = \frac{f_{e1} + f_{o1}}{2 \times ABW} \tag{3b}$$

Fig. 2(a) shows theoretically calculated frequency response of tunable filter using coupling matrix. As depicted in Fig. 2(a), the passband center frequency of BPF is tuned from 1.40 GHz to 1.84 GHz with constant 1-dB ABW of 85 MHz when even-and odd-mode resonant frequencies of dual-mode resonant frequencies varied. In addition, quasi-elliptic response is achieved by generating two TZs at lower and upper sides of passband.

Fig. 2(b) shows the theoretically calculated frequency responses according to different cross-coupling $M_{14} = M_{36}$. As value of $M_{14} = M_{36}$ is increased, TZs are moved close to passband. These results confirm that TZs frequencies can be located at any arbitrary frequencies by controlling value of $M_{14} = M_{36}$.

Fig. 1(b) shows circuit implementation of the proposed 6th-order tunable BPF using three synchronously tuned dual-mode resonators. The coupling between dual-mode resonators is implemented using series capacitor C_{a2} and shunt capacitor C_{b2}. Likewise, coupling between source/load and dual-mode resonators is implemented through series capacitor C_{a1} and shunt varactor diode C_{b1}. The TZs are generated through cross-coupling which is implemented using transmission line (TL) with characteristic admittance Y_b and length L_b. The detailed analysis of the proposed filter is described in the following sections.

b) Resonant frequencies of dual-mode resonator

Fig. 3(a) shows the proposed structure of a dual-mode resonator which comprises two TLs with characteristics admittance Y_1, length L_1 and L_2, varactor diode with a capacitance of C_v, and short-circuited shut stub TL with characteristic admittance Y_k and length L_k. Each dual-mode resonator combines two resonators. Using the even- and odd-mode equivalent circuits shown in Fig. 3(b) and 3(c), the even- and odd-mode input admittances are derived as (4).

$$Y_{ine} = jY_1 \frac{AY_1 \tan\beta L_1 - 1}{AY_1 + \tan\beta L_1} \tag{4a}$$

$$Y_{ino} = jY_1 \frac{\omega C_v (\tan\beta L_1 \tan\beta L_2 - 1) - Y_1 \tan\beta L_1}{\omega C_v (\tan\beta L_1 + \tan\beta L_2) - Y_1} \tag{4b}$$

where

$$A = \frac{2Y_1 \tan\beta L_k + Y_k \tan\beta L_2}{Y_1 Y_k - 2Y_1^2 \tan\beta L_k \tan\beta L_2} - \frac{1}{\omega C_v} \tag{5}$$

The even- and odd-mode resonant frequencies (f_e and f_o) can be extracted by setting $im(Y_{ine}) = 0$ and $im(Y_{ino}) = 0$. The center frequency and BW are predefined as $f_c = (f_e + f_o)/2$ and $f_{BW} \cong (f_o - f_e)$. To analyze corresponding response, we varied capacitance of varactor diode 1T362 from Sony Inc with C_v ranging from 2.8 to 50 pF.
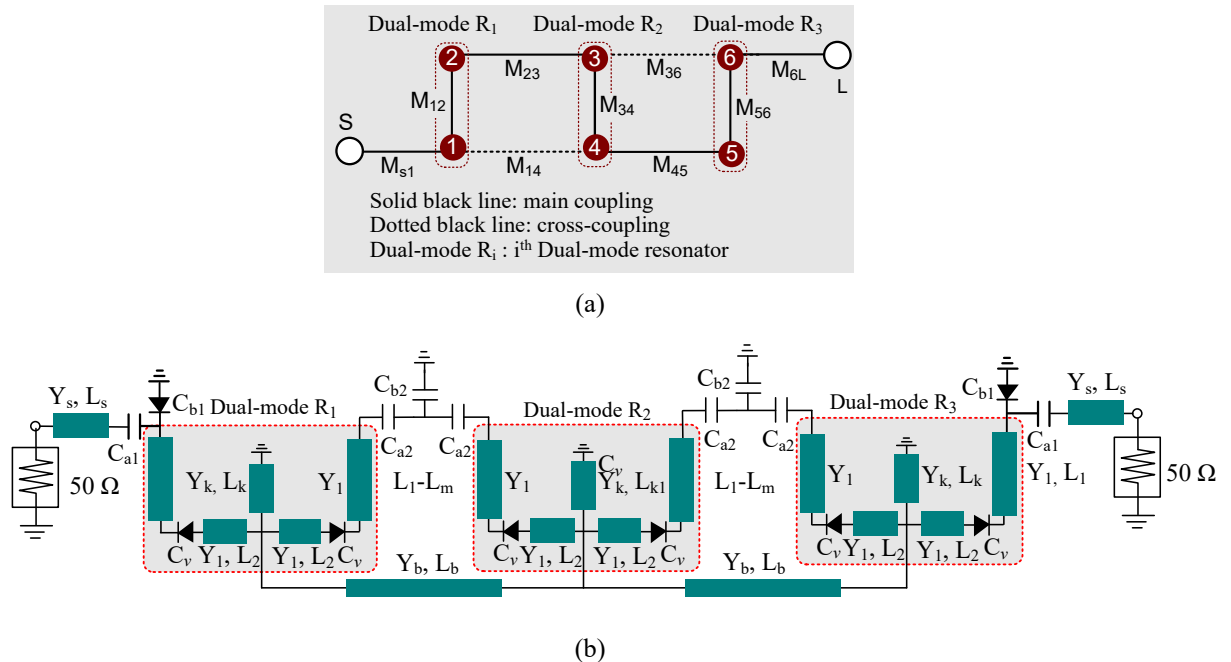

(a)

(b)

Fig. 1. (a) Coupling diagram of 6th-order tunable BPF with transmission zeros and (b) circuit implementation of 6th-order tunable BPF using three synchronously tuned dual-mode resonators.
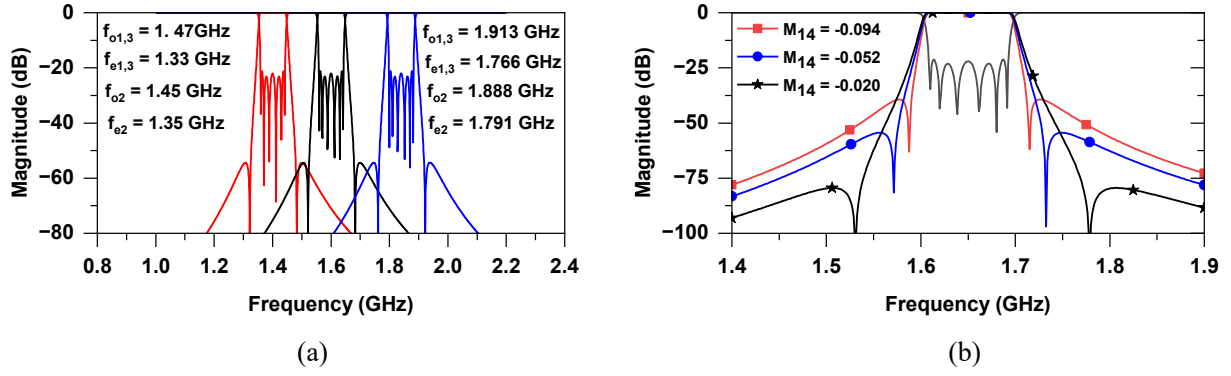
Fig. 2. (a) Theoretical design parameters and frequency responses of proposed 6th-order tunable BPF and (b) frequency responses according to different cross-coupling values. Coupling matrix: $M_{s1} = M_{6L} = 1.0394$, $M_{12} = M_{56} = 0.8650$, $M_{23} = M_{45} = 0.6451$, $M_{34} = 0.5732$, $M_{14} = M_{36} = -0.052$, and ABW = 85 MHz.
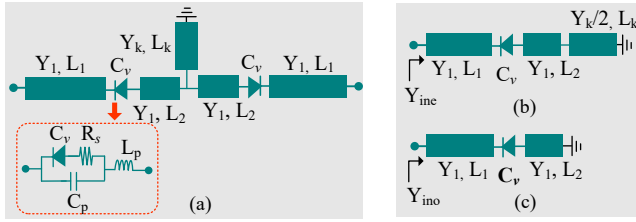

Fig. 3. (a) Proposed synchronously tuned dual-mode resonator, (b) even-mode equivalent circuit, (c) odd-mode equivalent circuit.

The f_e and f_o can be tuned by changing C_v as depicted in Fig. 4(a). Moreover, as illustrated in Fig. 4(b), the value of L_k has an impact on f_e and causes it to deviate away from f_o when L_k is increases. By selecting appropriate values L_k and L_1, nearly constant or decreasing f_{BW} can be achieved, as demonstrated in Fig. 4(c) and 4(d). Based on these analysis, tunable BPF with constant ABW can be realized using the proposed resonator.

c) Coupling between the dual-mode resonator

Fig. 1 shows the coupling diagram and circuit implementation of 6th-order tunable BPF using three synchronously tuned dual-mode resonators. To achieve constant ABW, the frequency-dependent coupling between dual-mode resonators is realized with a T-network consisting of series and shunt capacitors. Fig. 5(a) and 5(b) illustrate the coupling between dual-mode resonators and its equivalent inverter circuit model, which consists of series capacitors C_{a2} and shunt varactor capacitance C_{b2}. The series capacitor C_{a2} also acts as DC-block capacitor. The T-network (series C_{a2} and shunt C_{b2}) of each mode represents an admittance inverter $J_{i,i+1}$. Using circuit shown in Fig. 5(b), the values of admittance inverter $J_{i,i+1}$ is expressed as (6).

$$J_{i,i+1} = Y_1 \left| \tan\left\{ \beta L_m + \tan^{-1} \frac{\omega C_{a2} C_{b2}}{2Y_1 C_2 + Y_1 C_{b2}} \right\} \right| \tag{6}$$

where

$$L_m = -\frac{1}{2\beta} \tan^{-1} \left\{ \frac{2\omega C_{a2} Y_1 (C_{a2} + C_{b2})}{Y_1^2 (2C_{a2} + C_{b2}) - \omega^2 C_{a2}^2 C_{b2}} \right\} \tag{7}$$

If a negative value of L_m is obtained, it will be absorbed into the length of the dual-mode resonator. After obtaining value of admittance inverter value $J_{i,i+1}$ for given C_{a2} and C_{b2}, the coupling coefficient $k_{i,i+1}$ between dual-mode resonators can be calculated using (8).

$$k_{i,i+1} = \frac{J_{i,i+1}}{\frac{\omega_c}{2} \frac{\partial}{\partial \omega} \left\{ Im\left(\frac{Y_{ine} + Y_{ino}}{2} \right) \right\} \Big|_{\omega = \omega_c}} \tag{8}$$

where $\omega_c = 2\pi f_c = \pi(f_e + f_o)$. Using (6)-(8), Fig. 5(c) illustrates the calculated $k_{i,i+1}$ between dual-mode resonators with respect to C_{a2} and C_{b2}. The strength of $k_{i,i+1}$ increases as C_{a2} increases and C_{b2} decreases. Moreover, $k_{i,i+1}$ decreases almost linearly when the center frequency is increased from 1.40 GHz to 1.84 GHz. Therefore, the desired $k_{i,i+1}$ for constant ABW can be achieved by appropriately selecting C_{a2} and C_{b2}.

d) External Q-factor

Fig. 6(a) illustrates the circuit implementation of even-and odd-mode external Q-factors, which is comprised of fixed series capacitor C_{a1}, and shunt varactor diode capacitance C_{b1}. The series C_{a1} also functions as a DC-block capacitor. The addition of C_{a1} and C_{b1} results in a shift of resonant frequency of dual-mode resonators toward to lower frequency, and this effect can be compensated by decreasing length L_1 of dual-mode resonator. Using Fig. 6(a), the even and odd-mode input admittances at source/load ports can be calculated using (9).

$$Y_{inS}^{e,o} = jY_s \frac{Y_{ina}^{e,o} + \tan\beta L_s}{Y_s - Y_{ina}^{e,o} \tan\beta L_s} \tag{9}$$
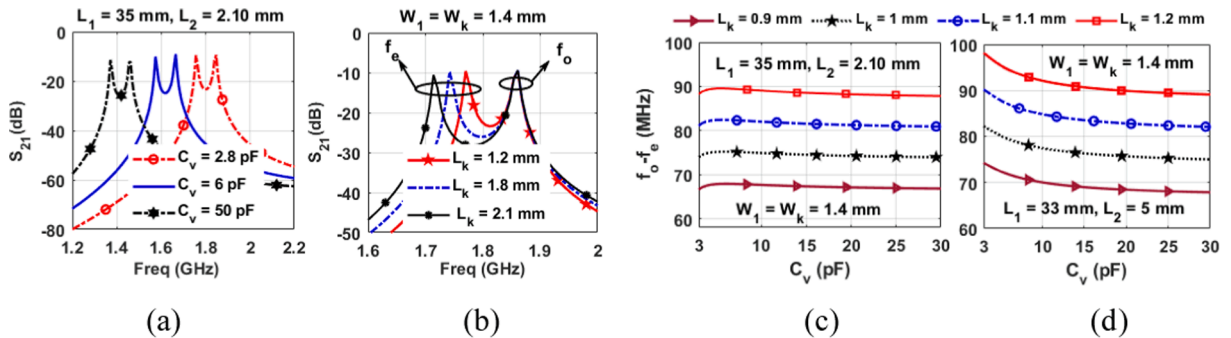

Fig. 4. (a) Resonant frequency variation of dual-mode resonator with C_v, (b) even-mode resonant frequency variation with L_k, (c) constant bandwidth, and (d) decreasing bandwidth with varication of C_v.
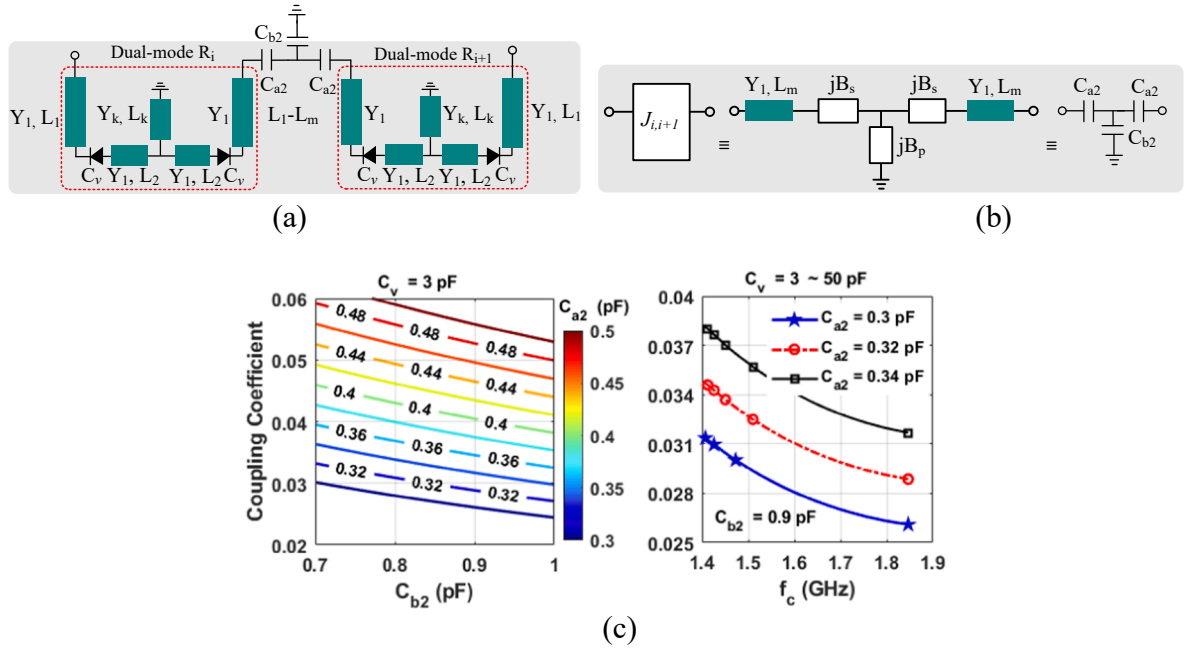
Fig. 5. (a) Coupling between dual-mode resoantors, (b) equivalent addittance inverter model, and (c) calculated coupling coefficient according to C_{a2}, C_{b2} and C_v.
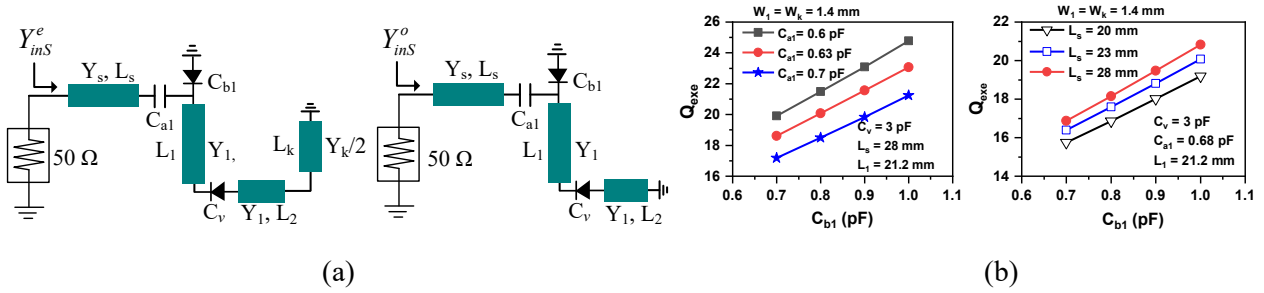

Fig. 6. (a) Structure of even- and odd-mode external Q-factor and (b) calculated external Q-factor according to C_{a1}, C_{b1} and L_s.

where

$$Y_{ina}^{e,o} = \frac{\omega C_{a1} Y_{in}^{e,o}}{\omega C_{a1} + Y_{in}^{e,o}}, Y_{in}^o = \omega C_{b1} + B \quad (10a)$$

$$Y_{in}^e = \omega C_{b1} + Y_1 \frac{A Y_1 \tan\beta L_1 - 1}{A Y_1 + \tan\beta L_1} \quad (10b)$$

$$B = Y_1 \frac{(\omega C_v \tan\beta L_2 - Y_1)\tan\beta L_1 - \omega C_v}{\omega C_v \tan\beta L_2 + \omega C_v \tan\beta L_1 - Y_1} \quad (10c)$$

and superscripts e and o denote even and odd-mode equivalent circuits. The value of A is same as (5). Using (9), the external Q-factor can be expressed as (11) where Q_{even} and Q_{odd} are even- and odd-mode Q-factors and $Z_0 = 1/Y_0 = 50\ \Omega$.

$$Q_{exe} = \frac{Q_{even} + Q_{odd}}{2} = \frac{\omega_e}{4Y_0} \frac{\partial Im\left[Y_{inS}^e(\omega_e)\right]}{\partial\omega}\bigg|_{\omega=\omega_e} + \frac{\omega_o}{4Y_0} \frac{\partial Im\left[Y_{inS}^o(\omega_o)\right]}{\partial\omega}\bigg|_{\omega=\omega_o} \quad (11)$$

The desired external Q-factor for designing tunable BPF with constant ABW can be obtained by trying different combination of C_{a1}, C_{b1} and L_s. Fig. 6(b) demonstrates the calculated external Q-factors with varying values of C_{a1}, C_{b1}, and L_s. When C_{a1} and L_s are fixed, increasing C_{b1} leads to linear increase in the external Q-factor. On other hand, a higher external Q-factor can be achieved by choosing smaller value of C_{a1} is

small, and larger value of L_s.

e) Design Example

As a design example, 6th-order tunable BPF is designed and simulated for constant ABW of 85 MHz and normalized transmission zero (TZ) frequencies of ± 2.10 rad/s. The microstrip line tunable BPF is designed and simulated using a substrate with a dielectric constant of 2.2 and thickness of 0.787 mm. The circuit parameters are obtained from the analysis discussed in previous sections. The simulation results are shown in Fig. 7, demonstrating excellent agreement with coupling matrix results. The designed BPF achieved a constant ABW of 84 ± 1.5 MHz when f_0 was tuned from 1.42 GHz to 1.84 GHz by tuning external Q-factors with help of shunt C_{b1}. The two TZ frequencies are located at the lower and upper sides of the passband and can be controlled by varying lengths of L_b. The higher filter-order and TZs provide high-frequency selectivity and large attenuation level in the stopband.

3. Experimental verification

To experimentally validate the design, a 6th-order tunable BPF was fabricated with a constant ABW of 85 MHz and FTR of 1.40 ~ 1.80 GHz. The BPF was implemented on a substrate with dielectric constant of 2.20 and thickness of 0.787 mm. Variable capacitances C_v and C_{b1} were realized using varactor diode 1T362 from Sony Inc., which provided diode capacitance between 3 pF and 100 pF by varying the reverse bias voltage between 30 V and 0 V [25]. Fig. 8(a) presents the physical layout of the 6th-order BPF including its physical dimensions, while the
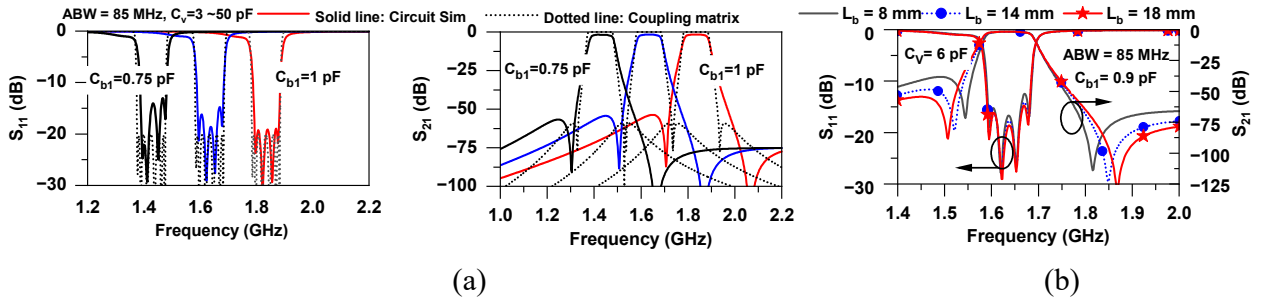
Fig. 7. (a) Simulation results of 6th-order tunable BPF with constant absolute bandwidth and (b) controllable TZs location according to L_b.
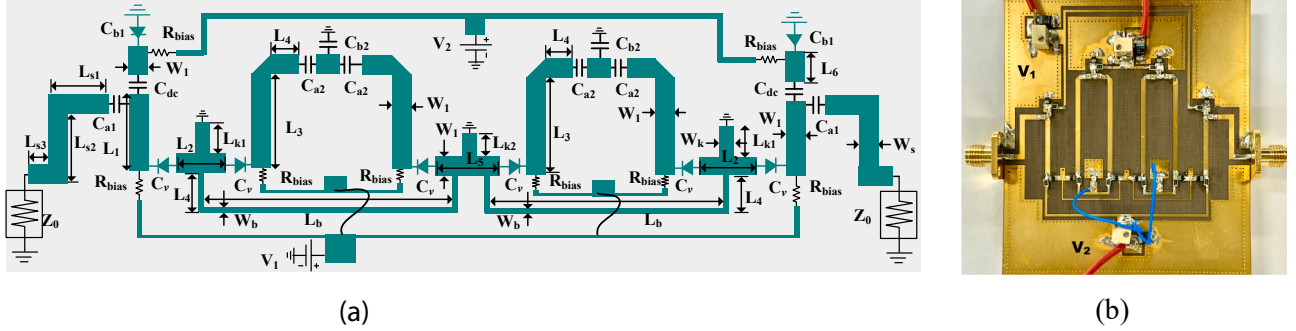

Fig. 8. (a) Physical layout (b) photograph of fabricated filter.

photograph of fabricated filter is shown in Fig. 8(b). The physical dimension of fabricated filter are given as: $W_s = 1.50$, $W_1 = W_k = 1.38$, $L_{s1} = 6.7$, $L_{s2} = 9.5$, $L_{s3} = 4.3$, $L_1 = 18.26$, $L_2 = 4.60$, $L_3 = 28$, $L_4 = 2$, $L_6 = 2.50$, $L_{k1} = 2.15$, $L_{k2} = 1.60$, $W_b = 0.4$, $W_b = 0.4$, $L_b = 18.8$, $C_{a1} = 0.75$ pF, $C_{dc} = 1$ pF, $C_{b2} = 2$ pF, $C_{a2} = 0.3$ pF, and $R_{bias} = 5$ kΩ and physical dimension unit is millimeter (mm). The simulation was performed using an equivalent circuit model of the varactor provided by the manufacturer [25]. The circuit parameters have been optimized using ANSYS HFSS and Keysight ADS.

The results of simulation and measurement are shown in Fig. 9, indicating that they are consistent with each other. The measured results confirmed that center frequency can be tuned from 1.39 GHz to 1.81 GHz while maintaining 1-dB constant ABW of 62 ± 1.5 MHz (60.5 ~ 63.5 MHz). The measured insertion loss (IL) varies from 6.42 dB to 6.95 dB; while return losses are better than 10 dB across the entire frequency tuning range. Two TZs are located at lower and upper sides of the passband. When the measuring input third-order intercept point (IIP3) using two-tone input signals separated by 1 MHz, IIP3 varied from 22.1 dBm to 34.90 dBm.

To investigate the cause of relatively higher IL, we have performed simulation of 6th-order tunable BPF using SPICE model of varactor diode 1T362 from Sony Corporation as shown in Fig. 10(a) and results are shown in Fig. 10(b). The IL is mainly due to parasitic resistance R_s of

varactor diode. The parasitic resistance R_s of varactor diode increases if dc-bias voltage of varactor diode is moved toward lower value (such as 0 V). Results shown in Fig. 10(b) confirm that the IL increases as the value of R_s increases. The IL of filter can be improved if varactor diode with low parasitic resistance (high Q-factor varactor diode) is used.

Table 1 presents a comparison of the performance of the proposed 6th-order tunable BPF with previously reported state-of-the-arts alternatives. Tunable BPF should provide large frequency tuning range (FTR), constant ABW, low passband IL, and high return loss (RL) characteristics within passband. However, it is very challenging to achieve the above required characteristics simultaneously. So, the trade-off among these characteristics of tunable BPF is necessary for optimum performance. Considering these characteristics, the figure of merit (FoM) of tunable BPF can be defined as (12)

$$FoM = \frac{FTR(MHz)}{ABW(MHz)} \times \frac{10^{\left(-\frac{IL_{\max}(dB)}{20}\right)}}{10^{\left(\frac{RL_{\min}(dB)}{20}\right)}} \qquad (12)$$

where $IL_{\max}$ and $RL_{\min}$ are maximum passband insertion loss and minimum return loss within entire frequency tuning range, respectively.

As shown in Table 1, the majority of the previously reported tunable BPFs that achieved constant ABW were 4th-order, with exceptions [23] and [24]. In [23], a 6th-order tunable BPF with a constant ABW of 40.8
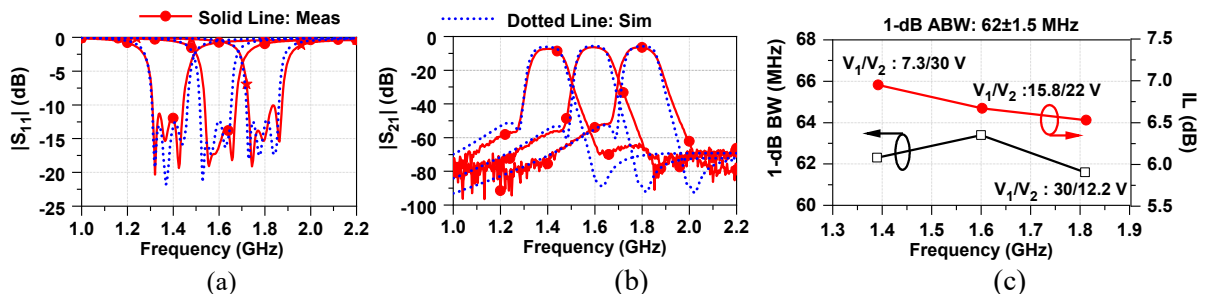

Fig. 9. Simulated and measured results: (a) $|S_{11}|$, (b) $|S_{21}|$, and measured insertion loss/bandwidth.
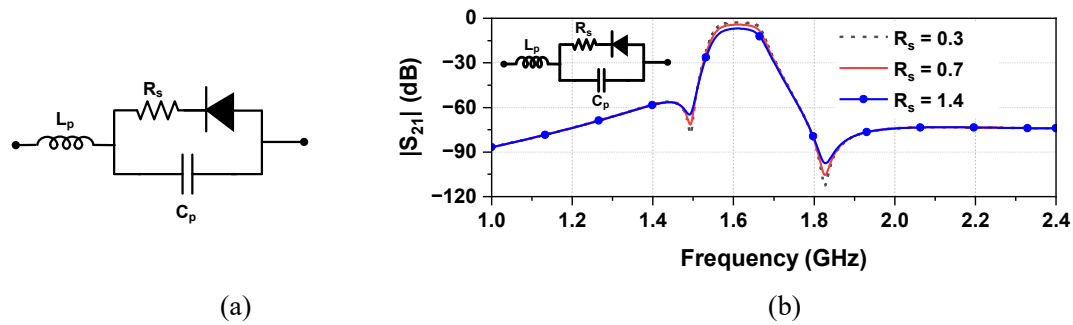
Fig. 10. Simulation results of proposed 6th-order according to parasitic resistance R_s of varactor diode: (a) equivalent SPICE model of varactor and (b) simulation results with different R_s. Other parasitic values of varactor diode: $L_s = 2$ nH, $C_p = 0.31$ pF [25].

Table 1
Performance comparison between this work and state-of-arts.

	Frequency tuning range: FTR (GHz)	IL_{max} (dB)	RL_{min} (dB)	1-dB ABW (MHz)	Filter order	No of bias	IIP3 (dBm)	*FoM*
[16]	1.25 ~ 2.10 (50.7 %)	< 8.50	>11	54 ~ 162	4	5	13 ~ 19	NA
[17]	0.97 ~ 1.53 (44.8 %)	< 4.20	>10.8	54 ~ 84	4	1	8 ~ 30.3	NA
[20]	0.95 ~ 1.48 (43.6 %)	< 4.40	>10	117 ± 3* (114 ~ 120)	4	2	22.9 ~ 34.9	8.63
[21]	1.24 ~ 1.72 (32.4 %)	< 5.40	>6	94.5 ± 2.5* (92 ~ 97)	4	2	12 ~ 21	5.44
[22]	1.05 ~ 1.40 (28.5 %)	< 3.50	>11	134 ± 1.5 (132.5 ~ 135.5)	4	2	16.3 ~ 29.95	6.19
[23]	0.88 ~ 1.12 (24.0 %)	< 7.10	>10	40.8 ± 2.4 (38.4 ~ 43.2)	6	1	NA	8.21
[24]	1.90 ~ 2.30 (19.5 %)	< 3.20	>9.8	580 ± 10 (570 ~ 590)	6	1	NA	1.47
This work	**1.39 ~ 1.81 (26.25 %)**	**< 6.95**	**>12**	**62 ± 1.50 (60.5 ~ 63.5)**	**6**	**2**	**22.1 ~ 34.90**	**12.12**

* 3-dB constant absolute bandwidth.

MHz was demonstrated, but the FTR of this design was 240 MHz (24 %), FTR/ABW = 5.88 and FoM = 8.21. Similarly, work [24] demonstrated 6th-order tunable BPF with FTR of 400 MHz (19.5 %), FTR/ABW = 0.69, and FoM = 1.47 only. In contrast, the proposed design achieves 1-dB constant ABW of 62 ± 1.5 MHz over wider FTR of 420 MHz (26.3 %), with FTR/ABW = 6.77, highest FoM, and exhibits excellent linearity characteristics.

4. Conclusion

This paper describes design of a higher-order tunable BPF with constant ABW and transmission zeros using synchronously tuned dual-mode resonators. The achievement of a constant ABW across a wide frequency tuning range is made possible through use of unique structural implementation of frequency-dependent couplings and tunable external quality factors. The simulation results are consistent with measurement results. The measured results confirmed that the proposed tunable BPF provides the highest figure of merit among the previously reported works. Furthermore, the proposed structure can be extended to higher than 6th-order, resulting in a 8th-order tunable BPF with constant ABW.

Declaration of Competing Interest

The authors declare that they have no known competing financial interests or personal relationships that could have appeared to influence the work reported in this paper.

Data availability

Data will be made available on request.

Acknowledgment

References

[1] Cameron RJ, Mansour R, Kudsia CM. Microwave Filters for Communication Systems: Fundamentals, Design and Applications. Hoboken, NJ, USA: Wiley; 2007.

[2] Lu D, Barker NS, Tang X. A simple frequency-agile bandpass filter with predefined bandwidth and stopband using synchronously tuned dual-mode resonator. IEEE Microw Wireless Compon Lett 2017;27(11):983–5.

[3] Lu D, Tang X, Barker NS, Feng Y. Single-band and switchable dual-/single-band tunable BPFs with predefined tuning range, bandwidth, and selectivity. IEEE Trans Microw Theory Techn 2018;66(3):1215–25.

[4] Mao JR, Choi WW, Tam KW, Che WQ, Xue Q. Tunable bandpass filter design based on external quality factor tuning and multiple mode resonators for wideband applications. IEEE Trans Microw Theory Techn 2013;61(7):2574–84.

[5] Kumar N, Narayana S, Sing YK. Constant absolute bandwidth tunable symmetric and asymmetric bandpass responses based on reconfigurable transmission zeros and bandwidth. IEEE Trans Circ Syst-II: Express Briefs 2022;69(3):1014–8.

[6] Lim T, Anand A, Chen J, Liu X, Lee Y. Design method for tunable planar bandpass filters with single-bias control and wide tunable frequency range. IEEE Trans Circ Syst-II: Express Briefs 2021;68(1):221–5.

[7] Fan M, Song K, Fan Y. Reconfigurable bandpass filter with wide-range bandwidth and frequency control. IEEE Trans Circ Syst-II: Express Briefs 2021;68(6):1758–62.

[8] Zakharov A, Rozenko S, Ilechenko M. Varactor-tuned microstrip bandpass filter with loop hairpin and combline resonators. IEEE Trans Circ Syst-II: Express Briefs 2019;66(6):953–7.

[9] Tang S, Li Z, Tang X, Liu Y, Cai Z, Luo J. A low-loss three-pole frequency-agile bandpass filter with constant absolute bandwidth. IEEE Int Microw Symp Dig 2019.

[10] Huang X, Feng Q, Zhu L, Xiang Q, Jia D. Synthesis and design of tunable bandpass filters with constant absolute bandwidth using varactor-loaded microstrip resonator. RF Microw Comput-Aided Eng 2014;24(6):681–9.

[11] Pandit N, Pathak NP. Center frequency and BW reconfigurable multi-mode bandpass filter with independently tunable TZs. IET Microw Antennas Propag 2019;13(10):1610–9.

[12] Zhou Z, Xiao F, Cao Y, Zhang Y, Tang X. Third-order bandwidth-tunable bandpass filter with two transmission zeros. Proc Asia Pacific Microw. Conference, 2018, 1480–1482.

[13] Li Z, Tang X, Liu Y, Luo J. Low-loss wide-tuning range three-pole frequency-agile bandpass diplexer with identical constant absolute bandwidth. IEEE Access 2019: 149833–45.

[14] Lee HM, Rebeiz GM. A 640–1030 MHz four-pole tunable filter with improved stopband rejection and controllable bandwidth and transmission zeros. IEEE Int Microw Symp Dig 2013:1–3.

[15] Chiou YC, Rebeiz GM. Tunable 1.55–2.1 GHz 4-pole elliptic bandpass filter with bandwidth control and >50 dB rejection for wireless systems. IEEE Trans Microw Theory Techn 2013;61(1):117–24.

[16] Yang T, Rebeiz GM. Tunable 1.25–2.1-GHz 4-pole bandpass filter with intrinsic transmission zero tuning. IEEE Trans Microw Theory Techn 2015;63(5):1569–78.

[17] Gao L, Rebeiz GM. A 0.97–1.53-GHz tunable four-pole bandpass filter with four transmission zeroes. IEEE Microw Wireless Compon Lett 2019;29(3):195–7.

[18] Chiang CT, Chen CF, Wang BH, Chen HY, Tsai Y-F, Yu HY, Li WJ. A miniaturized fully tunable quasi-elliptic bandpass filter. Proc Asia-Pacific Microw Conference, 2022; 530-532.

[19] Lin W, Lee TH, Wu K. Fully reconfigurable dual-mode bandpass filter. IEEE Int Microw Symp Dig 2018:397–400.

[20] Tian D, Feng Q, Xiang Q. Synthesis applied 4th-order constant absolute bandwidth frequency-agile bandpass filter with cross-coupling. IEEE Access 2018;6:72287–94.

[21] Lu D, Tang XH, Li M, Barker NS. Four-pole frequency agile bandpass filter with fully canonical response and constant ABW. IEEE Int Microw Symp Dig 2018:1–4.

[22] Lu D, Yu M, Barker NS, Li Z, Li W, Tang X. Advanced synthesis of wide-tuning range frequency-adaptive bandpass filter with constant absolute bandwidth. IEEE Trans Microw Theory Techn 2020;67(11):4362–75.

[23] Ohira M, Hashimoto S, Ma Z, Wang X. Coupling-matrix based systematic design of single-DC-bias controlled microstrip higher order tunable bandpass filters with constant absolute bandwidth and transmission zeros. IEEE Trans Microwave Theory Techn 2019;67(1):118–28.

[24] Huang X, Zhang J, Lin Y, Xiang Q. Design of a six-pole tunable bandpass filter with constant absolute bandwidth. Proc Prog Electromagn Res Symp (PIERS), 2016; 3507–3510.

[25] T362: Silicon Variable Capacitance Diode, Sony Corporation.